J Fluoresc (2009) 19:955–966
DOI 10.1007/s10895-009-0495-6

ORIGINAL PAPER

Studying the Interaction of Pirarubicin with DNA and Determining Pirarubicin in Human Urine Samples: Combining Excitation -Emission Fluorescence Matrices with Second-order Calibration Methods

Hong-Yan Zou · Hai-Long Wu · Yan Zhang · Shu-Fang Li · Jin-Fang Nie · Hai-Yan Fu · Ru-Qin Yu

Received: 30 December 2008 / Accepted: 5 June 2009 / Published online: 7 July 2009
© Springer Science + Business Media, LLC 2009

Abstract In this paper, UV–vis spectroscopy and fluorescence were combined to study the binding of Calf thymus DNA (ct-DNA) with the anthacycline antibiotic drug pirarubicin (THP). Ethidium bromide (EB) as the fluorescence probe was used to study the competitive binding interactions of THP with DNA by excitation -emission fluorescence matrices (EEFMs) coupled with the parallel factor analysis (PARAFAC) and the alternating normalization-weighted error algorithm (ANWE) with the second-order advantage. All the results conformed that THP mainly bound with DNA by intercalation. Meanwhile, the two second-order calibration methods have been successfully applied to quantify THP in urine samples. Figures of merit were applied to compare the performance of the two methods. The results presented in this work showed that both the PARAFAC and ANWE methods were the convincing way to be applied in the complex biological systems even in the presence of uncalibrated interferences.

Keywords Pirarubicin · Ethidium bromide · DNA · PARAFAC · Second-order calibration

H.-Y. Zou · H.-L. Wu (✉) · Y. Zhang · S.-F. Li · J.-F. Nie · H.-Y. Fu · R.-Q. Yu
State Key Laboratory of Chemo/Biosensing and Chemometrics, College of Chemistry and Chemical Engineering, Hunan University, Changsha 410082, P. R. China
e-mail: hlwu@hnu.cn

Introduction

Pirarubicin (4′-O-tetrahydropyranyladriamycin, or THP) (Fig. 1a), a derivative of doxorubicin, is an anthracycline antibiotic developed during a search for less cardiotoxic agents among the 4′-O-substituted anthracyclines [1]. THP has been proved effective against hematological malignancies and was used for treatment of acute leukemias and malignant lymphomas, as well as breast cancer [2, 3]. The drug has both lipophilic and hydrophilic properties, which allows either intravenous or intra arterial injection with lipiodol used as a carrier for treatment of liver metastasis and hepatocellular carcinoma [4]. Unfortunately, THP lacks specificity for cancer cells, and its potent cytotoxicity, like that of many other low-molecular-weight cytotoxic anticancer agents, leads to severe side effects. Since DNA is an important cellular receptor, THP likes many chemicals through binding to DNA exert their antitumor effects. Therefore, the changing of DNA replication and the inhibiting growth of the tumor cells, which is the basis of designing new and more efficient antitumor drugs and their effectiveness depend on the mode and affinity of the binding [5, 6]. The mode of THP binding to DNA is still somewhat unclear, but is generally thought to involve binding to DNA by intercalation and inhibition of DNA biosynthesis, interference with topoisomerase II, and induction of DNA double strand breaks like doxorubicin and daunorubicin [7–11].

The binding interactions of small molecules with DNA have been studied extensively with a variety of techniques, including UV [12], isothermal calorimetric titration [13], quartz crystal microgravimetry [14, 15], mass spectrometry [16, 17], luminescence [18, 19], electrophoresis [20, 21],

NMR [22], fluorescence [23–26] and infrared spectroscopy [27]. With the development of high-order analytical instruments and trilinear chemometric algorithms, it becomes easier to obtain and resolve multi-dimensional data from complex systems [28–30]. The combination of three-dimensional EEFMs and second-order calibration methods could provide a powerful tool for studies of parallel competitive binding reactions of many chemical components with DNA in the presence of interferents. Such studies would be very helpful for understanding binding interactions of many drugs used in combination in the clinical treatment of some diseases [31–34]. Using second-order calibration methods such as the parallel factor analysis (PARAFAC) and the alternating normalization-weighted error algorithm (ANWE) with the so-called second-order advantage [35–37], makes it possible to determine the reaction pattern of different interacting pairs in a mixture medium.

In this work, UV–vis spectroscopy and fluorescence were combined to study the binding of ct-DNA with THP. The fluorescence of ethidium bromide (EB) (Fig. 1b) bound to ct-DNA was altered by THP in a dynamic way. The competitive binding interactions of THP and the fluorescence probe EB with DNA have been studied by excitation–emission fluorescence spectra to obtain a three-dimensional response data array. Second-order calibration methods based on the parallel factor analysis (PARAFAC) and the alternating normalization-weighted error algorithm (ANWE) were used to resolve the data array obtained.

Determination of THP in biological fluids has only been reported using separations methodologies, but these are relatively time-consuming and laborious [38, 39]. Their direct measurement in urine samples by EEFMs combined with the PARAFAC and ANWE methods can be an attractive alternative, due to its high sensitivity (SEN) and selectivity (SEL), and second-order advantage properties.

Trilinear component model

The PARAFAC model, which is also known as the name trilinear decomposition, has been proposed by Harshman [35] and Carroll and Chang [36]. It has different types of notation. The most usual type notation can be expressed as following form:

$$x_{ijk} = \sum_{n=1}^{N} a_{in} b_{jn} c_{kn} + e_{ijk} \quad (1)$$
$$\mathrm{i} = 1, 2, \ldots, \mathrm{I}; \mathrm{j} = 1, 2, \ldots, \mathrm{J}; \mathrm{k} = 1, 2, \ldots, \mathrm{K}$$

In this paper, the three-way data array $\underline{X}$ owes to excitation–emission matrix (EEM) fluorescence on I excitation wavelengths and J emission wavelengths for K samples for its consistency with Beer's law in chemistry. x_{ijk} represents a fluorescence intensity element; N denotes the number of factors, which should correspond to the total number of detectable species, including the component(s) of interest and the background as well as unknown interference(s); e_{ijk} is an element from the residual array $\underline{E}$; a_{in} and b_{jn} are the normalized intensities at the emission wavelength i and the excitation wavelength j, and c_{kn} is the relative concentration of component n in the k-th sample. The column vectors a_n, b_n and c_n are collected into the corresponding loading matrices A, B and C. The trilinear model is found to minimize the sum of squares of the residuals e_{ijk} in the model.

For the model above, Harshman [35] and Carroll and Chang [36] have proposed an alternating least squares approach (ALS) to solve the above-mentioned problem. ALS at first assumes the loading matrices in two modes and then estimates the unknown parameters of the third mode. This is advantageous because the algorithm is simple to implement, and simple to incorporate constraints in, and because it guarantees convergence. Kiers et al. [40] have

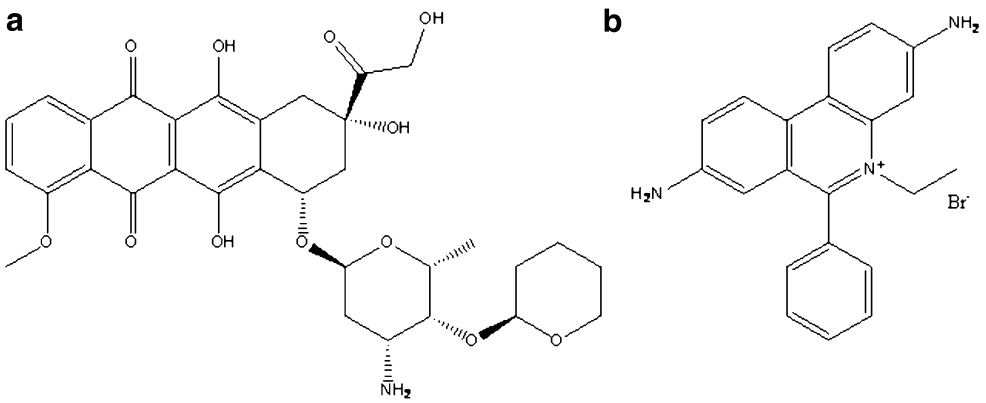

Fig. 1 Chemical structures of pirarubicin (**a**) and ethidium bromide (**b**)

developed the algorithmic shortcuts and expressed all the three sub-problems in term of the frontal slices of $\underline{X}$. This algorithm is computationally more efficient and the three updating steps for each mode are not identical. The general PARAFAC-ALS algorithm can be written as follows:

(1) Estimate the number of components N;
(2) Initialize A and B;
(3) Estimate C from $X_{..k}$, A and B

$$c^{T}_{(k)} = \left(A^{T}A * B^{T}B\right)^{-1} \mathrm{diag}\left(A^{T}X_{..K}B\right), \quad k = 1, 2, \ldots, K;$$

(4) Estimate A from $X_{..k}$, C and B:

$$A = \left(\sum_{k=1}^{K} X_{..k}B\,\mathrm{diag}\left(c_{(k)}\right)\right)\left(\sum_{k=1}^{K} \mathrm{diag}\left(c_{(k)}\right)B^{T}B\,\mathrm{diag}\left(c_{(k)}\right)\right)^{-1};$$

(5) Estimate B from $X_{..k}$, A and C:

$$B = \left(\sum_{k=1}^{K} X_{..k}A\,\mathrm{diag}\left(c_{(k)}\right)\right)\left(\sum_{k=1}^{K} \mathrm{diag}\left(c_{(k)}\right)A^{T}A\,\mathrm{diag}\left(c_{(k)}\right)\right)^{-1};$$

(6) Return to step (3), until convergence.

$X_{..k}$ is the kth slice of $\underline{X}$;c(k) is the the kth row of C;diag ($c_{(k)}$) denotes the diagonal of order NxN, with elements of the vector $c_{(k)}$. The superscript T denotes the transpose of a matrix.

After finishing the iterative procedure, if the columns corresponding to the components of interest in the finally obtained estimates of A, B, and C have been appropriately post-processed according to the uniqueness property, the physical significance of A, B, and C can be more easily understood. The final concentration estimates in unknown samples may be obtained by regression of relative concentration contributions of each component of interest against its standard concentrations in the calibration samples.

The PARAFAC model is sensitive to the estimated component number in one system. Either over-estimation or under-estimation of the underlying factors will result in erroneous results. The true underlying spectra will be received if the data is indeed trilinear and the right number of components is used. In this paper the core consistency diagnostic, which was proposed by Bro et al. [41], has been chosen to estimate the number of underlying factor.

In order to overcome the problems occurred in practical situations of PARAFAC analysis, Xia *et al.* [37] presented the ANWE algorithm, which was performed by utilizing alternating least-squares principle and the alternating normalization-weighted error to minimize three different objective functions simultaneously. The authors indicated that the model could avoid the two-factor degeneracy, relieve the slow convergence problem, and be insensitive to the estimated component number.

Figures of merit

For comparison of the performance of various methods, the figures of merit such as limit of detection, sensitivity and selectivity etc. are employed regularly. In our study the calculations of the sensitivity and selectivity [42, 43] in the article are adopted, where the equation is

$$\mathrm{SEN} = k_n \left\{ \left[\left(A^{T}A\right) \cdot \left(B^{T}B\right)\right]^{-1} \right\}_{nn}^{-1/2} \tag{2}$$

Selectivity is the ratio between sensitivity and total signal. So the selectivity can be simply obtained by dividing the Eq. (2) by k_n. Limit of detection (LOD) [44] can be calculated as

$$\mathrm{LOD} = 3.3_{s0} \tag{3}$$

Here s0 is the standard deviation of the concentration estimated for 3 different blank samples.

Experiment

Materials

THP and ct-DNA (Calf thymus DNA) was purchased from Sigma, America. EB (ethidium bromide, 95%) was purchased from J&K Chemical Ltd, Sweden. All the materials were used as purchased and no further purification was carried out. At 260 and 280 nm, the absorbance ratio of solution ct-DNA in Tris–HCl [tris-(hydroxy methyl) amino-methanehydrogen chloride] buffer solution (pH 7.4, 1.0 M) equaled to 1.8:1, which indicated that the DNA was sufficiently free of protein. The DNA concentration per nucleotide was determined by absorption spectra using the molar absorption coefficient (6600 $M^{-1}cm^{-1}$) at 260 nm [45]; its stock solution was 1.27×10^{-4}M. A 2.41×10^{-4}M stock solution of EB was prepared by dissolving 5 mg of its crystals in doubly distilled water, and diluted to 50 ml. A 3.18×10^{-5}M stock solution of THP was prepared by dissolving 2 mg of its crystals in doubly distilled water

and diluted to 100 ml. A 1.0 M Tris–HCl buffer (pH 7.4) was prepared for adjusting and diluting the test samples. Blank urine was obtained from fresh people and stored at −20°C. All the chemicals used were of analytical grade reagents, and doubly distilled water was used throughout.

Apparatus

Electronic absorption spectra of DNA binding studies were recorded on a Shimadzu UV-1501 multi spectrophotometer using 1.0 cm quartz cells. All the fluorescence spectra were recorded by a Hitachi F-4500 fluorescence spectrophotometer with the use of a 1.0 cm quartz cell. The PARAFAC-ALS and ANWE programs compiled in MATLAB were used to resolve the spectra and relative concentrations of the compounds in equilibrious mixtures. All calculations were carried out on a PC under the Windows XP operating system.

Procedure

Spectroscopic studies

Electronic absorption spectra of THP were recorded in the absence and presence of increasing amount of ct-DNA in Tris–HCl buffer solution of pH 7.4.

Emission fluorescence spectra of THP were recorded in the absence and presence of ct-DNA (λ_{ex}=500 nm, λ_{em}=550 nm). Emission fluorescence spectra of EB and system containing constant concentration of EB and ct-DNA were also recorded while varying the concentration of THP (λ_{ex}=490 nm, λ_{em}=590 nm).

Chemometric studies

Two groups of reaction solutions were prepared. One reaction solutions was prepared by adding the constant concentration of EB but varying concentration of ct-DNA into 5 ml volumetric flasks as in Table 1. The other reaction solutions were prepared by adding the constant concentration of EB and ct-DNA but varying concentration of THP into 5 ml volumetric flasks as in Table 2. All Binding reaction took place at the temperature of 25°C. The three-dimensional EEFMs were recorded after the equilibrium of complex reaction was reached with the slit widths of 5 nm, and a scan wavelength speed of 2400 nm min^{-1}. To avoid the Rayleigh scattering, the same range of excitation and emission wavelengths for the two system were 418–518 nm and 542–660 nm, with a scan wavelength intervals of 2 nm, we got two three-way arrays: 60×51×4 and 60×51×7 ($\lambda_{em}\times\lambda_{ex}\times$samples) respectively. Tris–HCl buffer of pH 7.4 was used as blank solution and subtracted. The spectra as well as concentrations of the complexes in the equilibrious mixtures all were resolved by the PARAFAC-ALS and the ANWE algorithm compiled in MATLAB.

Table 1 EB and DNA concentrations ($\times10^{-6}$M) of the samples of Nos. 1–4

Sample Nos	1	2	3	4
EB	1.21	1.21	1.21	1.21
DNA	0	3.18	6.56	8.94

Table 2 EB, DNA and THP concentrations ($\times10^{-6}$M) of the samples of Nos. 5–11

Sample Nos	5	6	7	8	9	10	11
EB	3.32	3.32	3.32	3.32	3.32	3.32	3.32
DNA	0	6.56	6.56	6.56	6.56	6.56	6.56
THP	0	0	1.18	4.72	6.36	14.21	17.64

Determination of pirubicin in urine samples

Appropriate volumes of working solution of THP (3.18×10 −5 M) and 2 ml of the urine were mixed and added to 10 ml volumetric flasks and diluted to the mark with doubly distilled water. To avoid the Rayleigh scattering, The ranges of excitation and emission wavelengths for urine samples were 400–499 nm and 515–650 nm with a scan wavelength intervals of 3 nm at the scan rate of 2400 nm min^{-1} to form a 46×34×13 ($\lambda_{em}\times\lambda_{ex}\times$sample) array. The doubly distilled water as the reagent blank was subtracted. Table 3 listed the concentration of THP in the calibration set and prediction set.

Results and discussion

Spectroscopic studies of the interaction with DNA

Ultraviolet–visible spectroscopy was a method for judging the affinity of small molecules with DNA. The binding of certain complex to DNA produced hypochromism, a broadening of envelope and a red shift of the complex absorption band. These effects were particularly pronounced for intercalators with groove binder, a large wavelength shift usually correlated with a complex conformational change on binding or complex–complex interactions. The calf thymus DNA had absorption at 260–280 nm and THP had absorption at 480–550 nm. Therefore, DNA was added directly to the THP solution, which was used to

Table 3 Results for THP in spiked urine samples obtained with PARAFAC and ANWE models for samples of Nos. 12–24 (μg ml^{-1})

Calibration set		Prediction set			
sample	Added	sample	Added	Predicted	
				PARAFAC	ANWE
12	1.10	19	0.60	0.597(99.5)	0.580(96.7)
13	1.40	20	0.80	0.752(94.0)	0.739(92.4)
14	1.60	21	1.60	1.471(91.9)	1.469(91.8)
15	2.00	22	1.80	1.744(96.9)	1.746(97.0)
16	2.80	23	2.00	2.041(102.1	2.048(102.4)
17	4.00	24	2.40	2.490(103.4)	2.50(104.1)
18	4.80				
Average recovery (%)				98.0±6.1	97.4±5.0

examine the reaction of DNA with THP by the change of the absorption of THP. The absorption spectral changes of THP with addition of DNA were shown in Fig. 2. The absorption spectra of THP exhibited a broad maxima peak in the range 490–500 nm. The addition of ct-DNA to the solution of THP resulted in a decrease in the absorption followed by a little red shift (496 to 498 nm) of absorption maxima, indicating a shift to a more polar environment on interaction. This result was a typical characteristic of intercalation mode [46, 47] involving a strong stacking interaction between the aromatic chromophore region of the complex and the base-pairs of DNA.

Fluorescence emission spectra of THP were recorded in the absence and presence of DNA. The excitation wavelength was fixed at 500 nm. With the addition of DNA, the fluorescence intensity of THP decreased (Fig. 3) which also indicated that the compound may bind with DNA by intercalation.

Fluorescence quenching can be dynamic, resulting from collisional encounters between the fluorophore and quencher, or static, resulting from the formation of a ground state complex between the fluorophore and quencher, which gave information about the changes of the molecular microenvironment in a vicinity of the chromophore molecules and the binding to DNA. Static and dynamic quenching can be distinguished by their different binding constants which were dependent on temperature and viscosity, or preferably by lifetime measurements. In this paper, we have used the binding constants dependence on the temperature and lifetime measurements to elucidate the quenching mechanism. The well-known Stern–Volmer equation [48] can be applied to confirm the mechanism.

$$\frac{F_0}{F} = 1 + K_{SV}[Q] = 1 + K_q\tau_0[Q] \quad (4)$$

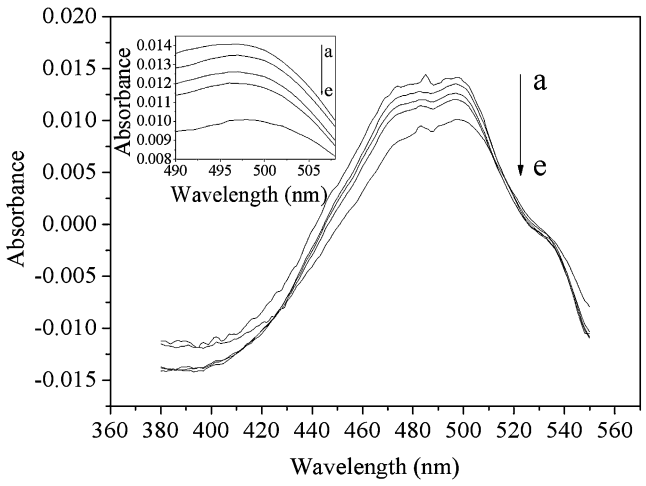

Fig. 2 UV–vis spectra of THP in the absence and presence of ct-DNA: C_{THP}=3.18×10^{-6}M and C_{DNA}=0 M (a), 6.36×10^{-6}M (b), 1.59×10^{-6}M (c), 4.77×10^{-6}M (d), 1.91×10^{-6}M (e)

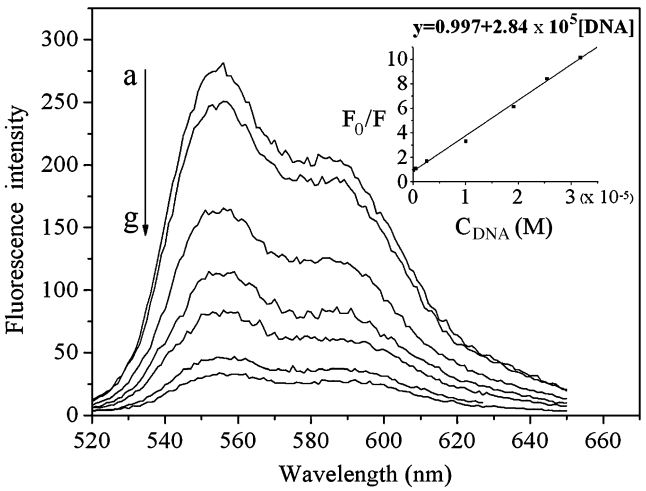

Fig. 3 Changes in fluorescence emission spectra of THP with increasing concentration of ct-DNA: C_{THP}=6.36×10^{-6}M and C_{DNA}=0 M (a), 4.36×10^{-7}M (b), 2.52×10^{-6}M (c), 1.02×10^{-5}M (d), 1.91×10-^{5}M (e), 2.54×10^{-5}M (f), 3.18×10^{-5}M (g)

Where F_0 and F were the fluorescence intensities in the absence and presence of quencher, respectively, k_q the biomolecular quenching constant, τ_0 the life time of the fluorescence in absence of quencher, [Q] the concentration of quencher, and K_{SV} was the Stern–Volmer quenching constant. Herein, Eq. (4) was applied to determine K_{SV} by a linear regression of the plot of F_0/F against [Q] at different temperature as in Fig. 4. The value of Ksv decreases obviously along with the temperature increased. The values of k_q ($2.87\times10^{13}M^{-1}s^{-1}$ at 298 K) was larger than the limiting diffusion constant K_{dif} of the biomolecular ($K_{dif}=2.0\times10^{10}M^{-1}s^{-1}$), which suggested that the fluorescence quenching was caused by a specific interaction between THP and ct- DNA. The quenching mechanism was mainly arisen from the predominant of complexes formation, while dynamic collision could be negligible in the concentration studied and they formed a non-fluorescenct ground state complex [48]. The quenching data must be analyzed according to the modified Stern–Volmer equation [49]:

$$\frac{F_0}{\Delta F}=\frac{F_0}{F_0-F}=\frac{1}{f_aK_a}\frac{1}{[Q]}+\frac{1}{f_a} \quad (5)$$

In this case, ΔF was the difference in fluorescence in the absence and presence of the quencher at concentration [Q], f_a was the fraction of accessible fluorescence and Ka was the effective quenching constant for the accessible fluorophores. The dependence of $\frac{F_0}{\Delta F}$ on the reciprocal value of the quencher concentration 1/[Q] was the linear with slope equal to the value of $1/f_aK_a$ as in Fig. 5. The value of $1/f_a$ was fixed on the ordinate. The constant Ka was the quotient of an ordinate $1/f_a$ and slope$1/f_aK_a$. The f_a was 0.94 and the binding constant Ka was $3.4\times10^5M^{-1}$.

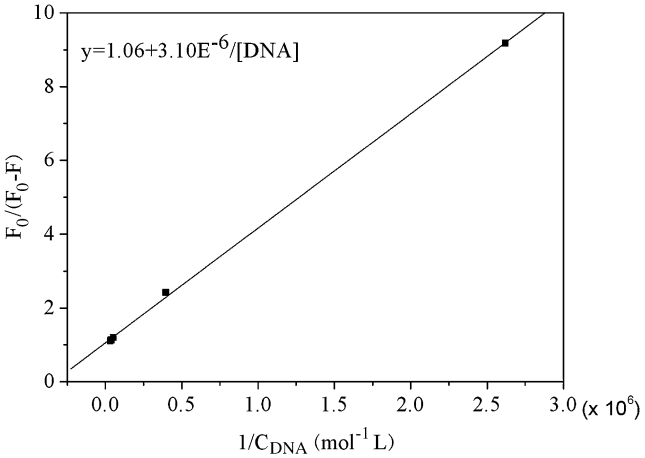

Fig. 5 Modified Stern–Volmer plot for THP with increasing concentration of ct-DNA

Ethidium bromide (EB) was one of the most sensitive fluorescence probes having a planar structure that binds DNA by an intercalative mode [47]. The fluorescence of EB highly increased after DNA intercalation and as shown in Fig. 6. However, the enhanced fluorescence can be quenched evidently when there was a second complex that can replace the bound EB or break the secondary structure of DNA [50]. When THP was added into the EB-DNA solution, their fluorescence intensity increased regularly with the increasing concentration of THP at the emission wavelength 590 nm, and there was a new increasing peak at 550 nm, which was the emission wavelength of THP. Because the fluorescent spectra of THP and EB, EB-DNA overlapped seriously, we can not get enough information

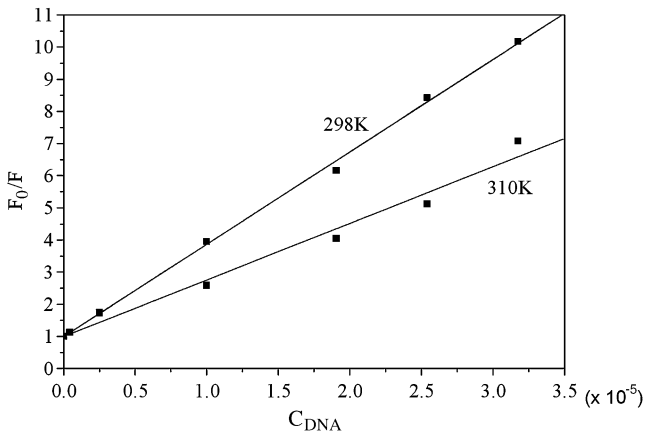

Fig. 4 Stern–Volmer plots for THP with increasing concentration of DNA

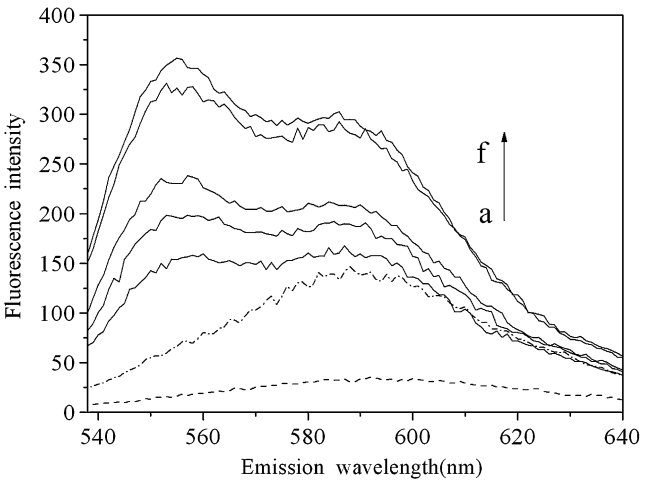

Fig. 6 Fluorescence intensity of 2.41×10^{-6}M EB (…),EB-DNA (- - -) ($C_{DNA}=6.35\times10^{-6}$M) and presence of THP at different concentration from a-f (—): 0 M (**a**), 1.18×10^{-6}M (**b**), 2.36×10^{-6}M (**c**), 3.18×10^{-6}M (**d**), 4.7×10^{-6}M (**e**), 5.88×10^{-6}M (**f**)

from the changes of fluorescence intensity. But we can see cleanly the changes of the fluorescent spectra for the mixtures of EB, EB-DNA and THP from fluorescence contour plot (Fig. 7a, b). It showed the presence of new bilateral peaks (see arrows, Fig. 7b) around λ_{ex}=500 nm and the peak around λex=520 nm disappeared (see arrows, Fig. 7a). This indicated that there were interactions between the compounds and significant overlapping among their spectra. The fluorescence spectra from the EB-DNA-THP mixture contain information ascribed to interactions among the components as well as spectral overlapping; thus, not all the peaks for all components would be represented on the contour plot with some fluorescence peaks being superimposed and submerged. Therefore, it became difficult to select the optimal excitation wavelength for further investigations of this complex mixture. Consequently, instead of the two-way EEM used for the contour work, three-way EEM array stacks were generated from the complex fluorescence systems, and were submitted to second-order calibration analysis to extract more information.

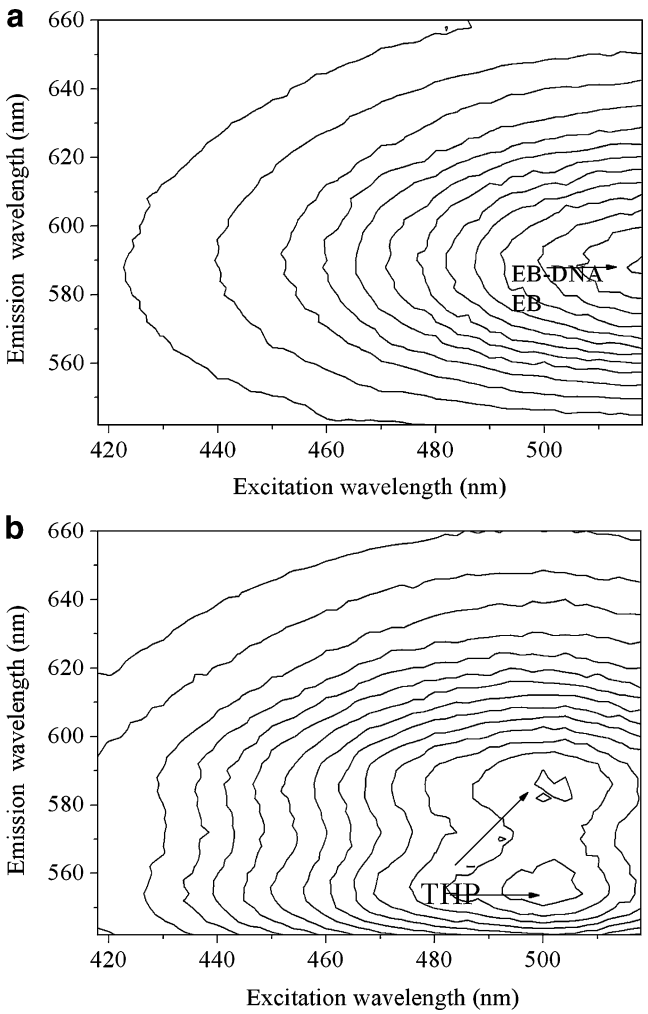

Fig. 7 The fluorescence contour plots for mixtures of EB, EB-DNA (**a**) and the mixtures of EB, EB-DNA and THP (**b**)

Studies of the interactions with DNA by second-order calibration methods

With the development of chemometric algorithm for higher order data, in particular for the trilinear excitation-emission fluorescence data array, it became possible to study the interactions of drugs with DNA by second-order calibration methods. From these methods, one can directly obtain the DNA binding modes without utilizing Scatchard plot, as well as the equilibrium concentrations of all fluorescing chemicals with a proper intensity.

As EB-DNA was a complex formed in the equilibrious mixtures of EB and DNA, It was difficult to get its true pure spectra .To obtain the underlying true spectra of EB-DNA, the PARAFAC and ANWE models were applied to the 60×51×4 three way array.

Excitation and emission spectra of EB resolved by PARAFAC and ANWE models using component two were shown in Fig. 8. It can be seen that the resolved EB spectra matched the recorded ones well. EB that intercalated into DNA formed a fluorescent complex EB-DNA and the resolved relative concentration values changed accordance with reference [48]. The concentrations of two components resolved by the two models took on the same changing trends. We can conclude the other spectra belonged to complex EB-DNA.

When we turned to the 60×51×7 three-way array, the excitation and emission spectra of EB, EB-DNA, and THP resolved by PARAFAC and ANWE models using component three were shown in Fig. 9a. It can be seen that all the resolved spectra matched the recorded ones well. That the concordance of the resolved three spectral profiles corresponding to the three components with the excitation and emission spectra of EB-DNA, EB and THP, confirmed that the resolved concentration values corresponding to these components were relative concentrations of EB, EB-DNA, and THP in corresponding reaction mixtures (Fig. 9b). The concentrations of three components resolved by the two algorithms took on the same changing trends. It can be seen that the relative concentration of EB decreased and EB-DNA increased initially accordance with Fig. 8b. With the concentration of THP increased, the relative concentration of EB-DNA decreased and the relative concentration of EB increased gradually. One can assume that the interaction of THP and EB with DNA possessed a competitive mechanism. That was, the interactions were a pair of the parallel competitive reactions. The results above conformed well to the results of Fig. 2 and Fig. 3.

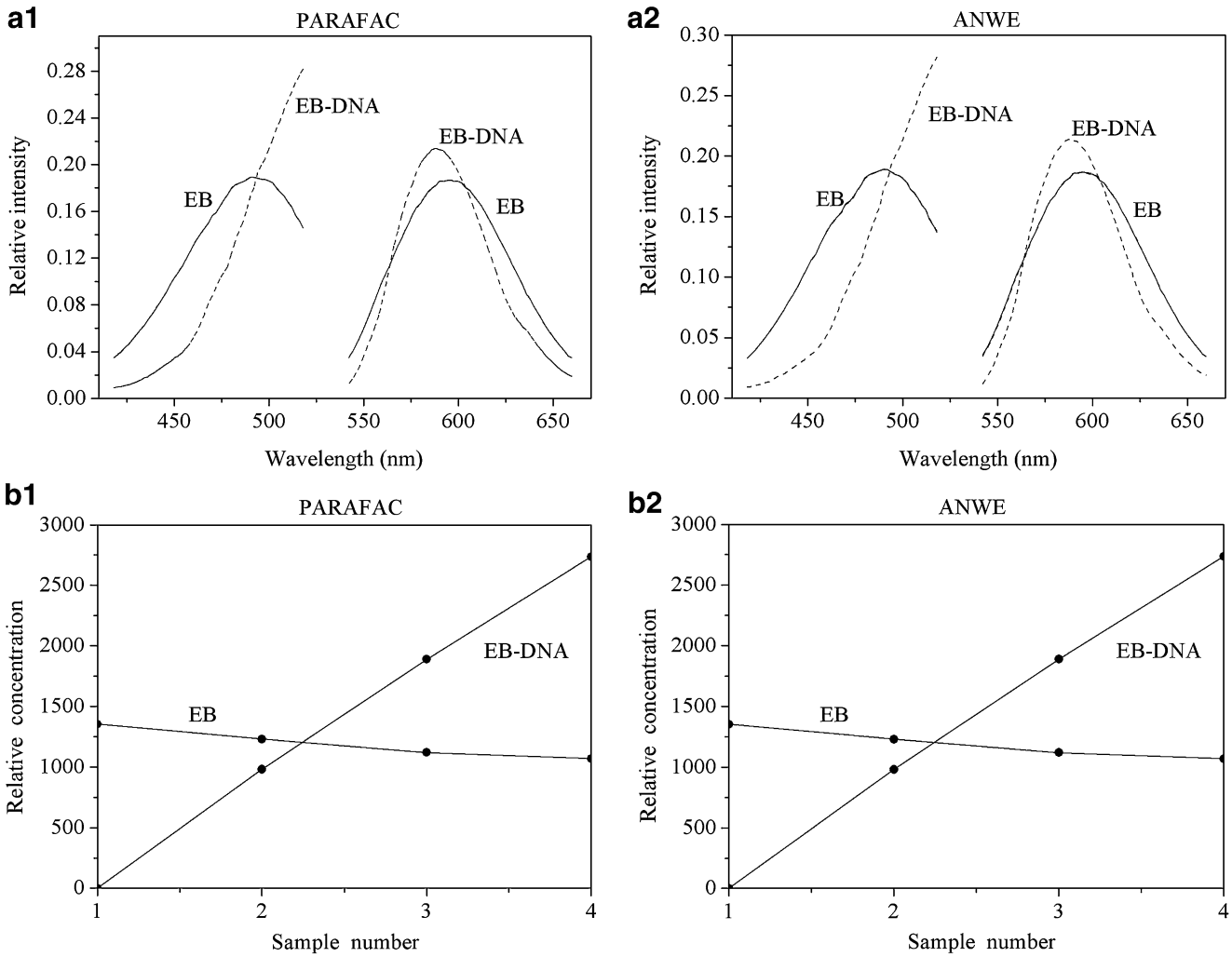

Fig. 8 Excitation–emission spectral (**a**) and relative concentration profiles (**b**) of each component using the PARAFAC and ANWE models when the chosen factor number are two for samples 1–4. Solid and dashed lines were the recorded and resolved spectra, respectively, of EB-DNA and EB

Determination of THP in urine samples by second-order calibration methods

The main advantage of second-order calibration was that it allowed spectral and concentration information for an individual component to be extracted even in the presence of unknown components. Thus, it was especially useful for resolving mixtures of components or for determining single components in complex samples like urine, where many compounds may be present.

The emission and excitation spectral profiles provided by PARAFAC and ANWE models using component two when the urine samples were processed together with the calibration set (Fig. 10). It was clear that, in the presence of urine matrices, the profiles resolved by the PARAFAC and ANWE models nicely matched those measured for the pure THP solution. The concentration predicted was seen in Table 3. The recovery of 99.8% with PARAFAC and 97.4% with ANWE were found. It should be considered to be satisfactory considering the complex components in urine, meaning that the second-order advantage has been exploited and the two second-order calibration methods was a creditable method to compensate for the complex mixtures.

The root-mean-square error of prediction (RMSEP) can be calculated in terms of the formula as $\mathrm{RMSEP} = \left[\frac{1}{I-1}\sum_{i=1}^{I}\left(c_{act}-c_{pre}\right)^2\right]^{1/2}$ where I was the number of prediction samples, c_{act} and c_{pred} were the actual and predicted concentrations of the analytes, respectively. The RMSEP results and the figures of merit, including SEN, SEL, LOD and the correlation coefficient (R) for direct quantification

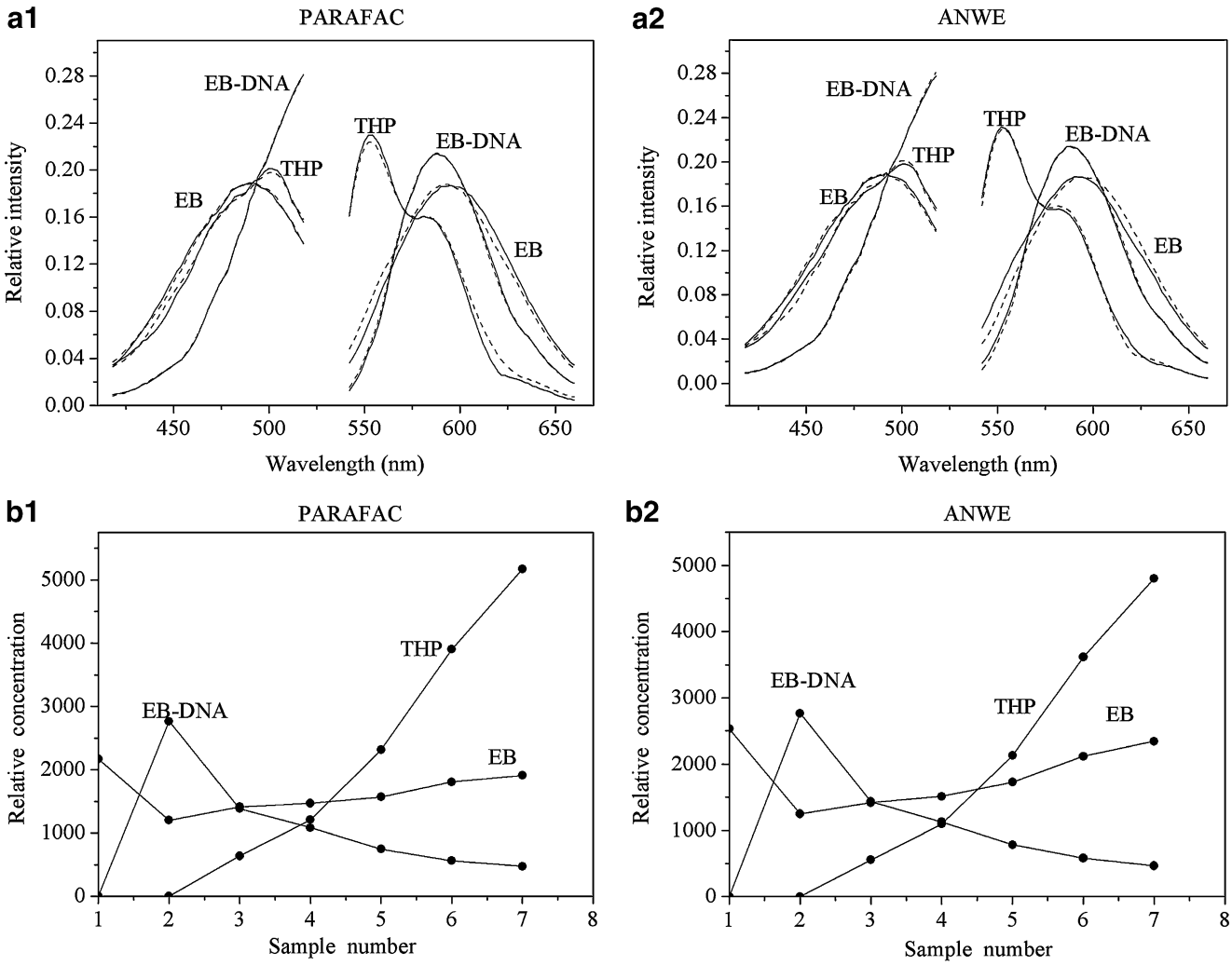

Fig. 9 Excitation–emission spectral (**a**) and relative concentration profiles (**b**) of each component using the PARAFAC and ANWE models when the chosen factor number were three. Solid and dashed lines were the recorded and resolved spectra, respectively, of EB-DNA, EB and THP

of pirorubicin in urine were shown in Table 4. The similar results were found for the figures of merit by the two models. Nevertheless, a greater sensitivity with slight lower LOD and RMSEP were found with the PARAFAC model.

Moreover, a linear-regression analysis of the actual versus the predicted concentration was applied to further investigate the accuracy of the two proposed algorithms of PARAFAC and ANWE. The calculated intercept and slope were compared with their ideal values of 0 and 1, based on the elliptical joint confidence region (EJCR) test [51]. If the point (0, 1) lay inside the EJCR, then bias were absent and consequently, the recovery may be taken as unity (or 100% in percentile scale). Figure 11 gave the results of EJCRs for both the PARAFAC and ANWE models. It shown that the ideal point (0, 1) labeled with a pentacle (☆) lay in all EJCRs .The elliptic size corresponding to the PARAFAC model was smaller than that related to the ANWE model. These results proved again that both models could allow for accurate quantitative determinations of THP in human urine, but the PARAFAC model was slight better in this system suffering from serious matrix effects.

Conclusion

In this paper, UV–vis spectroscopy and fluorescence were combined to study the binding of ct-DNA with THP. Competitive binding interactions of THP and the fluorescence probe EB with DNA have been studied by three-dimensional EEFMs combined with the PARAFAC and ANWE models. The relative equilibrium concentrations of EB-DNA, EB and THP in the equilibrium system can be

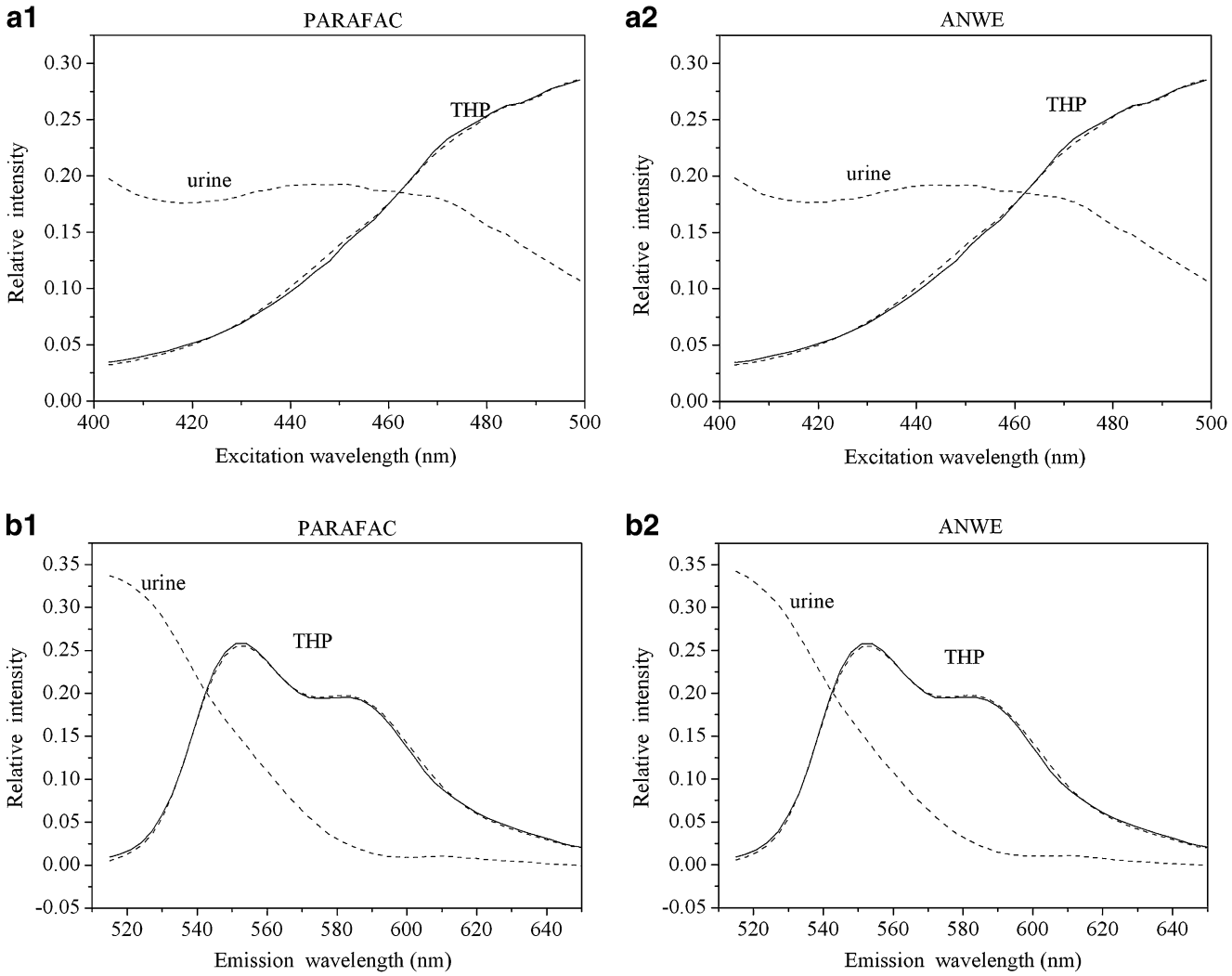

Fig. 10 Actual spectral profiles of THP (solid line) and resolved excitation–emission spectral (dashed line)each component using the PARAFAC and ANWE models when the chosen factor number was two in urine samples

directly obtained. All spectroscopic studies conformed that THP mainly bound with DNA by intercalation. A simple, rapid, and effective strategy has been successfully applied to quantify THP in urine samples by the PARAFAC and ANWE methods with the second-order advantage. But the PARAFAC method was slight better in this system

Table 4 Statistical parameters and figures of merit for the determination of THP in urine by PARAFAC and ANWE models

	PARAFAC	ANWE
RMSEP(μg ml^{-1})	0.0064	0.0073
SEN (ml μg $^{-1}$)	1489.7	1485.1
SEL	0.919	0.919
R	0.998	0.998
LOD(μg ml^{-1})	0.047	0.056

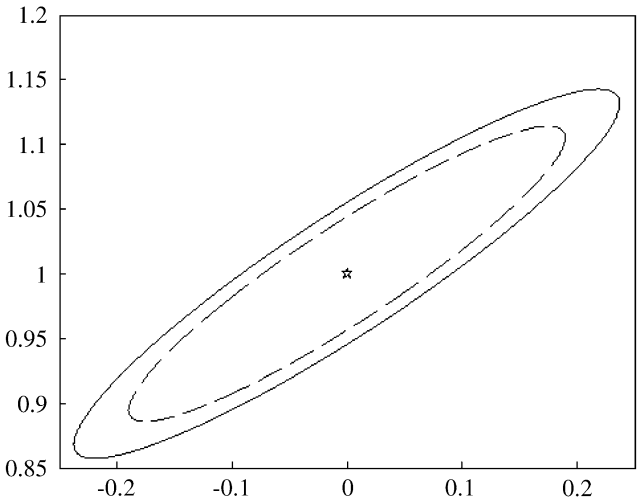

Fig. 11 EJCRs for THP in human urine applying PARAFAC and ANWE models.The dashed lines and solid lines corresponded to the EJCRs in human urine by PARAFAC and ANWE, respectively. The pentacle (☆) indicated the ideal points (0, 1)

suffering from serious matrix effects. It can be concluded that both two second-order calibration methods were the convincing way to be applied in the complex biological systems even in the presence of uncalibrated interferences.

Acknowledgements The authors would like to thank the National Nature Science Foundation of China (Grant Nos. 20775025 and 20435010) and the National 973 Project (2007CB216404) for financial supports.

References

1. Tsuruo T, Iida H, Tsukagoshi S, Sakurai Y (1982) 4′-O-tetrahydropyranyladr-amycin as a potential new antitumor agent. Cancer Res 42(4):1462–1467
2. Kimura K (1986) A phase II study of (2″R) - 4′-O-tetrahydropyranyladriamycin (THP) in patients with hematological malignancies. Jpn J Cancer Chemother 13(2):368–375
3. Enomoto K, Abe O, Tominaga T, Abe R, Iino Y, Koyama H, Fujimoto M, Nomura Y (1990) Clinical study of pirarubicin for breast cancer in Japan. Clinical Study Group of THP for Breast Cancer in Japan. J Clin Oncol 13(Suppl 1):S48–S53
4. Izumi N, Goto Y (1990) A clinical trial of transarterial chemoembolization for hepatocellular carcinoma using 4′-O-tetrahydropyranyladriamycin. Jpn J Cancer Chemother 17(7): 1303–1307
5. Carrasco C, Joubert A, Tardy C, Maestre N, Cacho M, Braña MF, Bailly C (2003) DNA sequence recognition by bispyrazinonaphthalimides antitumor agents. Biochemistry 42(40):11751–11761. doi:10.1021/bi034637h
6. Erdem A, Ozsoz M (2001) Interaction of the anticancer drug epirubicin with DNA. Anal Chim Acta 437:107–114. doi:10.1016/S0003-2670(01)00942-4
7. Pigram WJ, Fuller W, Hamilton LD (1972) Stereochemistry of intercalation: interaction of daunomycin with DNA. Nat New Biol 235(53):17–19. doi:10.1038/235017a0
8. Momparler RL, Karon M, Siegel SE, Avila F (1976) Effects of adriamycin on DNA, RNA and protein synthesis in cell-free systems and intact cells. Cancer Res 36(8):2891–2895
9. Tewey KM, Rowe TC, Yang L, Halligan BD, Lui LF (1984) Adriamycin-induced DNA damage mediated by mammalian DNA. topoisomerase II. Science 226(4673):466–468. doi:10.1126/science.6093249
10. Schneider E, Hsiang YH, Lui LF (1990) DNA topoisomerases as anticancer drug targets. Adv Pharmacol 21(1):149–183. doi:10.1016/S1054-3589(08)60342-7
11. Sander M, Hsieh TS (1983) Double stranded DNA cleavage by type II DNA topoisomerase from Drosophila melanogaster. J Biol Chem 258(13):8421–8428
12. Hutchins RA, Crenshaw JM, Graves DE, Denny WA (2003) Influence of substituent modifications on DNA binding energetics of acridine-based anticancer agents. Biochemistry 42(46):13754–13761. doi:10.1021/bi035434w
13. Lah J, Bezan M, Vesnaver G (2001) Thermodynamics of berenil binding to poly[d(AT)] poly[d(AT)] and poly[d(A)]poly[d(T)] duplexes. Acta Chim Slov 48(3):289–308
14. Su H, Williams P, Thompson M (1995) Platinum anticancer drug binding to DNA detected by thickness-shear–mode acoustic wave sensor. Anal Chem 67(5):1010–1013. doi:10.1021/ac00101a033
15. Aslanoglu M, Houlton A, Horrocks BR (1998) Functionalised monolayer for nucleic acid immobilisation on gold surfaces and metal complex binding studies. Analyst (Lond.) 123(4):753–757. doi:10.1039/a706897b
16. David WM, Brodbelt J, Kerwin SM, Thomas PW (2002) Investigation of quadruplex oligonucleotide-drug interactions by electrospray ionization mass spectrometry. Anal Chem 74 (9):2029–2033. doi:10.1021/ac011283w
17. Van Berkel GJ (2003) An overview of some recent developments in ionization methods for mass spectrometry. Eur J Mass Spectrom (Chichester, Eng.) 9(6):539–562. doi:10.1255/ejms.586
18. Rodriguez M, Bard AJ (1990) Electrochemical studies of the interaction of metal chelates with DNA. 4. Voltammetric and electrogenerated chemiluminescent studies of the interaction of tris(2,2′-bipyridine)osmium(II) with DNA. Anal Chem 62 (24):2658–2662. doi:10.1021/ac00223a002
19. Arkin MR, Stemp EDA, Turro C, Barton JK (1996) Luminescence quenching in supramolecular systems:A comparison of DNA- and SDS micelle-mediated photoinduced electron transfer between metal complexes. J Am Chem Soc 118(9):2267–2274. doi:10.1021/ja9532998
20. Okhonin V, Krylova SM, Krylov SN (2004) Nonequilibrium capillary electrophoresis of equilibrium mixtures, mathematical model. Anal Chem 76(4):1507–1512. doi:10.1021/ac035259p
21. Berezovski M, Krylov SN (2005) Thermochemistry of protein−DNA interaction studied with temperature-vontrolled nonequilibrium capillary electrophoresis of equilibrium mixtures. Anal Chem 77(5):1526–1529. doi:10.1021/ac048577c
22. Reynisson J, Schuster GB, Howerton SB, Williams LD, Barnett RN, Cleveland CL, Landman U, Harrit N, Chaires JB (2003) Intercalation of trioxatriangulenium ion in DNA:binding, electron transfer, X-ray crystallography, and electronic structure. J Am Chem Soc 125(8):2072–2083. doi:10.1021/ja0211196
23. McGhee JD, Von Hippel PH (1974) Theoretical aspects of DNA-protein interactions - cooperative and non-cooperative binding of large ligands to a one-dimensional homogeneous lattice. J Mol Biol 86(2):469–489. doi:10.1016/0022-2836(74)90031-X
24. Pachter JA, Huang CH, DuVernay VH, Prestayko AW, Crooke ST (1982) Viscometric and fluorometric studies of DNA interactions of several new anthracyclines. Biochemistry 21(7):1541–1547. doi:10.1021/bi00536a012
25. Mazerska Z, Dziegielewski J, Konopa J (2001) Enzymatic activation of a new antitumor drug, 5-diethylaminoethylamino-8-hydroxyimidazoacridinone, C-1311, observed after its intercalation into DNA. Biochem Pharmacol 61(6):685–694. doi:10.1016/S0006-2952(01)00527-5
26. Wang B, Bouffier L, Demeunynck M, Mailley P, Roget A, Livache T, Dumy P (2004) New acridone derivatives for the electrochemical DNA-hybridisation labeling. Bioelectrochem 63 (1–2):233–237. doi:10.1016/j.bioelechem.2003.10.020
27. Le Gal JM, Morjani H, Manfait M (1993) Ultrastructural appraisal of the multidrug resistance in K562 and LR73 cell lines from fourier transform infrared spectroscopy. Cancer Res 53(16):3681–3686
28. Rodríguez-Cuesta MJ, Boqué R, Rius FX, Picón Zamora D, Martínez Galera M, Garrido Frenich A (2003) Determination of carbendazim, fuberidazole and thiabendazole by three-dimensional excitation–emission matrix fluorescence and parallel factor analysis. Anal Chim Acta 491(1):47–56. doi:10.1016/S0003-2670(03)00786-4
29. Leitão JMM, Esteves da Silva JCG, Girón AJ, Muñoz de la Peña A (2008) Optimization of verapamil drug analysis by excitation-emission fluorescence in combination with second-order multivariate calibration. J Fluoresc 18(6):1065–1076. doi:10.1007/s10895-008-0351-0
30. Xia AL, Wu HL, Fang DM, Ding YJ, Hu LQ, Yu RQ (2006) Determination of daunomycin in human plasma and urine using an interference-free analysis of excitation-emission matrix fluorescence data with second-order calibration. Anal Sci 22(9):1189–1195. doi:10.2116/analsci.22.1189

31. Xie HP, Jiang JH, Cui H, Wu HL, Shen GL, Yu RQ (2002) Competitive interaction of the antitumor drug daunorubicin and the fluorescence probe ethidium bromide with DNA as studied by resolving trilinear fluorescence data: the use of PARAFAC and its modification. Anal Bioanal Chem 373(3):159–162. doi:10.1007/s00216-002-1306-y
32. Xie HP, Chu X, Jiang JH, Cui H, Shen GL, Yu RQ (2003) Competitive interactions of adriamycin and ethidium bromide with DNA as studied by full rank parallel factor analysis of fluorescence three-way array data. Spectrochimica Acta Part A 59 (4):743–749. doi:10.1016/S1386-1425(02)00224-X
33. Zhang F, Zhang QQ, Wang WG, Wang XL (2006) Synthesis and DNA binding studies by spectroscopic and PARAFAC methods of a ternary copper(II) complex. J PhotoChem & PhotoBio A Chemistry (Easton) 184(3):241–249
34. Ni YN, Lin DQ, Kokot S (2008) Synchronous fluorescence and UV–vis spectroscopic studies of interactions between the tetracycline antibiotic, aluminium ions and DNA with the aid of the Methylene Blue dye probe. Anal Chim Acta 606(1):19–25. doi:10.1016/j.aca.2007.10.051
35. Harshman RA (1970) Foundations of the PARAFAC procedure: models and conditions for an 'explanatory' multi-modal factor analysis. UCLA Working Papers in Phonetics 16(1):1–84
36. Carroll JD, Chang JJ (1970) Analysis of individual differences in multidimensional scaling via an N-way generalization of Eckart-Young decomposition. Psychometrika 35(3):283–319. doi:10.1007/BF02310791
37. Xia AL, Wu HL, Zhu SH, Han QJ, Zhang Y, Yu RQ (2008) Determination of psoralen in human plasma by using excitation-emission matrix fluorescence coupled to second-order calibration. Anal Sci 24(9):1171–1178. doi:10.2116/analsci.24.1171
38. Marchiset-Leca D, Leca FR (1993) Highly sensitive method for the determination of a new anthracycline: Pirarubicin. Chromatographia 35(7–8):435–438. doi:10.1007/BF02278598
39. Lachâtre F, Marquet P, Ragot S, Gaulier JM, Cardot P, Dupuy JL (2000) Simultaneous determination of four anthracyclines and three metabolites in human serum by liquid chromatography–electrospray mass spectrometry. J Chromatogr B Analyt Technol Biomed Life Sci 738(2):281–291. doi:10.1016/S0378-4347(99)00529-0
40. Kiers HAL, Krijnen WP (1991) Simple structure in component analysis techniques for mixtures of qualitative and quantitative variables. Psychometrica 56(1):147–152. doi:10.1007/BF02294592
41. Bro R, Kiers HAL (2003) A new efficient method for determining the number of components in PARAFAC modes. J Chemometr 17 (5):274–286. doi:10.1002/cem.801
42. Faber NM (2001) The price paid for the second-order advantage when using the generalized rank annihilation method (GRAM). J Chemometr 15(9):743–748. doi:10.1002/cem.688
43. Olivieri AC (2005) Computing sensitivity and selectivity in parallel factor analysis and related multiway techniques:the need for further developments in net analyte signal theory. Anal Chem 77(15):4936–4946. doi:10.1021/ac050146m
44. Boqué R, Ferré J, Faber NM, Rius FX (2002) Limit of detection estimator for second-order bilinear calibration. Anal Chim Acta 451(2):313–321. doi:10.1016/S0003-2670(01)01395-2
45. Reichmann ME, Rice SA, Thomas CA, Doty P (1954) A further examination of the molecular weight and size of desoxypentose nucleic acid. J Am Chem Soc 76(11):3047–3053. doi:10.1021/ja01640a067
46. Oliveira-Brett AM, Diculescu VC (2004) Electrochemical study of quercetin–DNA interactions: Part II. In situ sensing with DNA biosensors. Bioelectrochemistry 64(2):143–150. doi:10.1016/j.bioelechem.2004.05.002
47. Long EC, Barton JK (1990) On demonstrating DNA. Intercalation. Acc Chem Res 23(9):273–279. doi:10.1021/ar00177a001
48. Lakowicz JR (2006) Principles of Fluorescence Spectroscopy, 3rd edn. Springer, New York, pp 278–282
49. Lehrer SS (1971) Solute perturbation of protein fluorescence. Quenching of the tryptophyl fluorescence of model compounds and of lysozyme by iodide ion. Biochemistry 10(17):3254–3263. doi:10.1021/bi00793a015
50. Song YF, Yang P (2001) Mononuclear tetrapyrido[3, 2-a:2′, 3′-c:3′′, 2′′-h:2′′′, 3′′′-j]phenazine (tpphz) cobalt complex. Polyhedron 20 (6):501–506. doi:10.1016/S0277-5387(00)00648-3
51. González AG, Herrador MA, Asuero AG (1999) Intra-laboratory testing of method accuracy from recovery assays. Talanta 48 (3):729–736. doi:10.1016/S0039-9140(98)00271-9